International Journal of Science and Research (IJSR)
ISSN (Online): 2319-7064
Index Copernicus Value (2016): 79.57 | Impact Factor (2017): 7.296

Surface Morphology, Optical Conductivity, Localized States and Dielectric Constants of Sprayed Nickel Oxide Films at Different Substrate Temperatures

Alaa A. Akl[1, 2], Safwat A. Mahmoud[3], Salah M. M. Salman[4,5]

[1]Physics Department, Faculty of Science, Minia University, Minia, Egypt

[2]Physics department, Faculty of Science, Ed Dawadmi, Shaqra University, Saudi Arabia

[3]Physics Department, Faculty of Science, Northern Border University, Saudi Arabia

[4]Physics Department, Faculty of Science, Helwan University, Ain-Helwan-Egypt

[5]Educational Services, Qassim University, Ministry of High Education, Saudi Arabia

Abstract: ***Thin films of nickel oxide (NiO) were deposited on glass substrates at a different temperature of growth using a spray pyrolysis technique. X-ray diffraction (XRD) and optical properties have been studied for the properties of the samples obtained. Analysis of XRD data show that at a low growth temperature, an amorphous form has been obtained, while at high growth temperature ($T_{sub} \geq 275\ ^oC$), single phase of the NiO formed which has a cubic structure. Optical properties were examined using spectral measurement at wavelength range of 300-2500nm. Optical constants (n and k) were calculated from corrected transmittance and corrected reflectance. The data obtained show that the direct transition (Eg) decreased from 3.738 to 3.146 eV and the indirect transition change from 2.790 to 2.049eV with increasing temperature. On the contrary, Urbach energy (band tail width), E_U was found to be decreased from 0.65 to 0.36 eV. This behavior is believed to be associated with the increase of substrate temperatures. Optical conductivity, dielectric constants, optical density, skin depth, and electrical susceptibility were discussed as functions of substrate temperatures. From these results, NiO films has been categorized as an excellent material for optoelectronic applications and a potential candidate for solar cell applications because of its tune-ability for optimization.***

Keywords: Optical Conductivity, Dielectric Constant, Nickel Oxide, Thin Films, Spray Pyrolysis

1. Introduction

Optical properties are usually interpreted as the interaction between the photon incident and the material under study. The material can affect the characteristics of the incident beam, when passed by either transmission, absorption or reflection [1-3]. Therefore, the optical spectrum can give an overview of the physical process that occurs when interacting with light. In this context, optical absorption is an easy way to obtain band gap energy and explain the band structure of the material under study [3-4].The optical properties of thin films are very important for many applications, including interference devices (such as anti-reflective coatings, laser mirrors and monochromatic filters), optoelectronics, integrated optics, solar engineering, microelectronics and optical sensor technology [5-7]. Nanoparticles are known to exhibit interesting physical properties such as increasing the semiconductor band gap due to electron retention [8-11]. Surface atoms play an important role in controlling the electronic and optical properties of nanomaterial. Estimating the energy-band gap in semiconductors in nanostructures is somewhat difficult because the surface atoms in the valence and conduction bands are not surprising, and the tail cases complicate the definition of the real optical gap [1-8]. Nickel oxide is an important magnetic semiconductor with a wide gab 3.6eV and cubic crystal structure [1,2]. The promising candidate for many applications such as electro catalysis [3], the positive electrode in batteries [4], the fuel cells [5], the electrochromic devices [6], the solar thermal absorber [7] the catalyst for the evaluation of oxygen [8] and photo electrolysis [9]. Several physical and chemical methods, such as sputtering [10], pulse laser deposition [11], chemical bath deposition [10, 12], sol-gel [13], and spray pyrolysis [14,15] have been used to obtain nickel oxide films. All these methods offer different advantages depending on the application of interest, and many efforts have been made to obtain films with desired physical and/or chemical properties. Among the different methods of film deposition, the relative simplicity of a spray pyrolysis method and its potential application to deposit a large area make it very attractive, low cost and feasible for mass production processes.

In the previous two papers [14,15]; nickel oxide thin films were prepared on a heated glass substrate using spray pyrolysis of the nickel hydroxides $Ni(OH)_2$, NiOOH, to obtain films with different degrees of crystallization. The XRD study revealed the cubic structural modification of films deposited on heated substrates in the 350^oC with different solution molarity. The identification of the current phases showed the existence of a single phase of NiO polycrystalline. Single order Voigt profile method has been used to determine nanostructure parameters (crystallite size and microstrain) increased with increasing substrate

temperature. Dark conductivity at room temperature and activation energy of crystalline nickel oxide films was found to be $10^{-3}\Omega^{-1}.m^{-1}$ and 0.97eV, respectively. An analysis of the results showed that for NiO films, direct and indirect transitions occurred with the energies of 3.60 and 3.97eV, respectively. The refractive index depends on the thickness of the film and depends on the growth temperature. In this research, our previous study was completed by providing optical properties results obtained from amorphous and crystalline NiO thin films prepared on heated glass substrate by the spray pyrolysis method. Some important optical parameters such as optical absorption, complex refractive index, skin depth, Urbach energy (E_U), dielectric constant, optical density, optical conductivity and localized states were estimated and calculated. Analysis of the optical characteristic of nickel oxides naturally imposes application of the theoretical and experimental skills of micro-optics, interpretation and discussion.

2. Experimental details

Nickel oxide (NiO) thin films are prepared on the heated glass substrate at a different temperature. A 0.05M solution was prepared by dissolving 2.38g of nickel acetate tetra hydrate $Ni(CH_3COO)_2.4H_2O$ in 50 mL ethanol. It has passed through air sprays with a diameter of 0.7mm nozzle. The nitrogen flow rate was constant at 80 mL/hr and the spray rate of the solution was 70mL/hr. Aqueous solution after sprayed through an atomizer on heated glass substrates undergoes pyrolytic decomposition formation of thin film. Thermocouple has been used to measure substrate temperature. In order to explore the effect of substrate temperature ranging from 225 to 350^{o}C has been used to prepare these films. For a uniform thin film, a high spray nozzle, a molarity solution and the rate of spray operation remained constant during the deposition process at 35cm, 0.05M and 15cm^3/min, respectively. The atomic cross-section and surface roughness were carried out using atomic force microscope (AFM) (Park Scientific Instrument). Optical transmission and reflection of the films prepared over the wavelength of 250-2400nm using Shimadzu UV 3101 PC were recorded. UV-Vis-NIR Dual-beam spectrophotometer with reflective facility based on V-N geometry (angle of incident 5^{o}).

3. Results and Discussion

3.1 Morphological characterization

The root mean square of roughness (R_{RMS}) is a function that takes the measures square. The R_{RMS} roughness of a surface is similar to the average roughness, where the only difference is the absolute mean squared values of the roughness of the surface. All samples prepared using an atomic force microscope (AFM) were then scanned to obtain three-dimensional images of the surface topography that gave nanoscale information about the roughness of the film's structure. The following relationship was used to calculate the root mean square roughness (R_{RMS}) [16-18].

$$R_{RMS} = \sqrt{\frac{1}{N}\int_0^N |Z^2(x)|dx} \quad (1)$$

Where Z(x) is the function that describes the surface profile analyzed in terms of height (Z) and position (x) of the sample over the evaluation length "N". All the surface parameters are easily calculated in the AFM software. Figure 1 shows 3D AFM topography maps characterization of the prepared samples of NiO thin films at different substrate temperature. Investigated study of surface morphology observed that ordinates obey a normal distribution has been verified by observing the cumulative distribution of surfaces. For high temperature samples, this is physically reasonable since a large number of small particles of random shape achieved growth process. Therefore, the final distribution of the height of surface morphology was a combination of random growth and would follow the natural distribution according to the central reduction theory. At low substrate temperature, it can be seen that there are some beg particles size on the sample surface. Since the particles are very large, their effect was observed on microscale friction measurement. These particles are included in calculating surface roughness parameters. While at a higher temperature, it can be shown that the size of the small particles was displayed on the morphological surface.

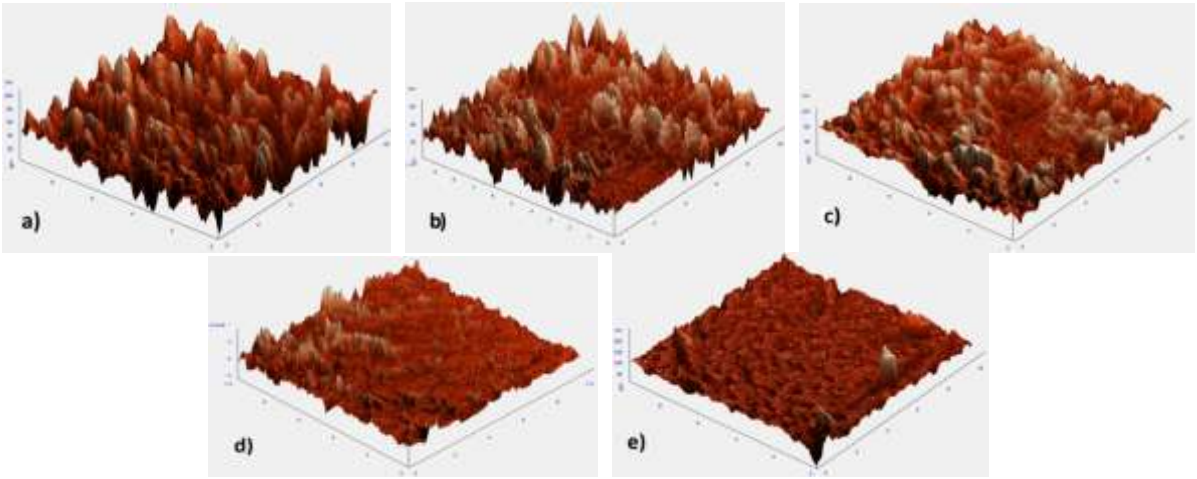

Figure 1: AFM micrographs images in 3D from NiO thin films at different substrate temperatures a) 225 ^{o}C, b) 250 ^{o}C, c) 275 ^{o}C, d) 300 ^{o}C and e) 350 ^{o}C

This is due to high friction forces between agglomeration particles for at low temperature samples. Table 1 shows root-mean-square (RMS) of roughness parameters measured for samples prepared [17,18]. Note that at lower temperature, the surface is distinctly rougher than the higher temperature. This is due to the large deviation of the skewness and the flattening of the Gaussian distribution may be caused by the inherent inefficiency of these parameters. Finally, it is clear that the assumption of an isotropic surface is valid for all surfaces of samples since directional patterns of AFM images can be investigated in the NiO thin films.

3.2 Optical characteristic study

3.2.1.Optical absorption coefficient

The spectral variation of the absorption coefficient versus the photon energy was calculated for NiO at different substrate temperatures as shown in Figure (2). On the absorption edge, suddenly rises to reach $1.0x10^5$ cm^{-1} observed values. Moreover, the absorptive edge of the higher temperature turns towards a shorter wavelength. The absorption coefficient was calculated based on the known relationship [19];

$$\alpha(\nu) = \frac{10^4}{d} Ln\left[\frac{1-R(\lambda)}{T(\lambda)}\right] \qquad (2)$$

Where R is the corrected reflectance, T is the corrected transmittance and d the thickness of the film.

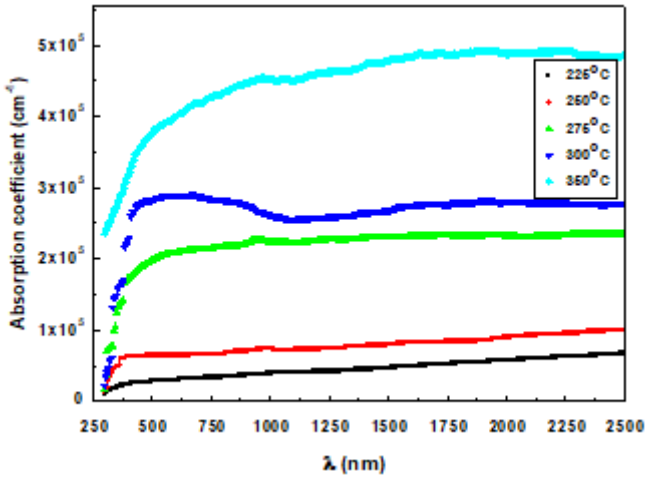

Figure 2: Coefficient of absorption, α of NiO thin films as a function of substrate temperature

Figure (2); indicates that the films examined have a higher absorption coefficient for all samples. Furthermore, the value of the absorption coefficient is clearly affected by structural film changes. It is clear that the absorption coefficients in the band edge areas are different, perhaps because the change in the composition of the NiO is not significant. On the other hand, the absorption coefficients at the upper substrate temperature in the midgap regions are higher than one lower temperature. These low absorption coefficients indicate a relatively low density of the medium, consistent with high transmission. These results indicate that there is no significant change in the density of the defect, which is also consistent with the photosensitivity saved around a single order of magnitude.

3.2.2. The skin effect and the skin depth

NiO films have a high optical absorption coefficient, and optical absorption change should be discussed in thin films. Photon energy absorbed into films depends on many parameters, such as the type of material, thickness, conductivity, and extinction coefficient of the films. There are some special and important parameters that are related to the absorption of photons within texture thin films, for example skin effect or skin thickness and optical conductivity. The current photon density is significantly reduced from the surface toward the middle of the film for many reasons, for example, film density, refractive index, surface morphology and microstructure of samples. The depth of the skin also depends on the conductivity of thin films and the frequency of incident photons. Since conductivity in semiconductors strongly depends on the optical band gap, one can associate optical properties and skin effect in any semiconductor material [20, 21]. The depth of the skin or penetration depth (δ) is related to the absorption coefficient (α) with the following simple relationship [20]:

$$\delta = 1/\alpha \qquad (3)$$

Figure 3 shows the depth of the skin, δ as a function of the wavelength of the beam falling on thin films of NiO at different temperatures. It is clear that the depth of the skin (δ) decreases with increasing both the substrate temperature and the wavelength. This is due to the behavior of the skin depth depends on the crystal structure of the film. Where the absorption coefficient is increasing as a function of the crystallization process and the reduced of the intensity and amplitude occurs after passing a small displacement. While, the skin depth will be increase in the amorphous structure, which indicates that the skin depth can be transmitted from the film. Similar results were obtained in the previse literatures [21-23].

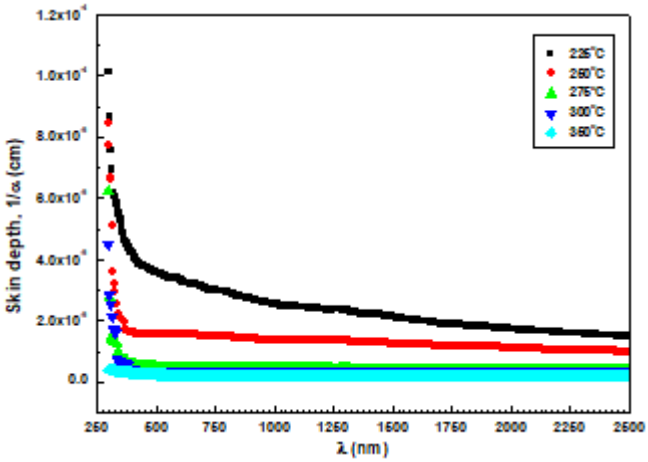

Figure 3: Variation of skin depth as a function of wavelength at different substrate temperatures.

3.2.3 Refractive index

A refractive index is one of the basic properties of optical materials, because it closes with respect to the electronic polarization of ions and the local field within the material. The complex optical constant (refractive index, n and extinction coefficient, k) was calculated for samples prepared from T(λ) and R(λ) corrected using a developed calculation program [24]. Both transmittance and reflection are given by Murmann's exact equations [19].

$$R(\lambda)=\frac{(n-1)^2}{(n+1)^2} \quad \text{And} \quad T(\lambda)=\frac{4n}{(n+1)^2} \qquad (4)$$

Where n is the real part of the refractive index of the thin film. However, when the film is absorbent, the reflection of R in the film's vacuum interface should take into account the value of k so that R can be written as Karmers – Kronig relationship [25];

$$R=\left[\frac{(n-1)^2+k^2}{(n+1)^2+k^2}\right] \qquad (5)$$

Spectral optical constants (n (λ) and k (λ)) can be calculated from spectral transmittance and experimental reflection using the Murmann's exact equation [19]. The behavior of the refractive index, n, has a higher value at a very low wavelength (strong absorption). This is due to the quality between the frequency of electromagnetic radiation incident and plasma frequency. Therefore, there is an abnormal dispersion of the refractive index in the plasma frequency region. However, when λ crosses λ_p (plasma wavelength) and the corresponding dielectric constant becomes negative, the refractive index becomes largely imaginary. Hence, there is no propagation of electromagnetic radiation through the medium and it is reflecting as mentioned above.

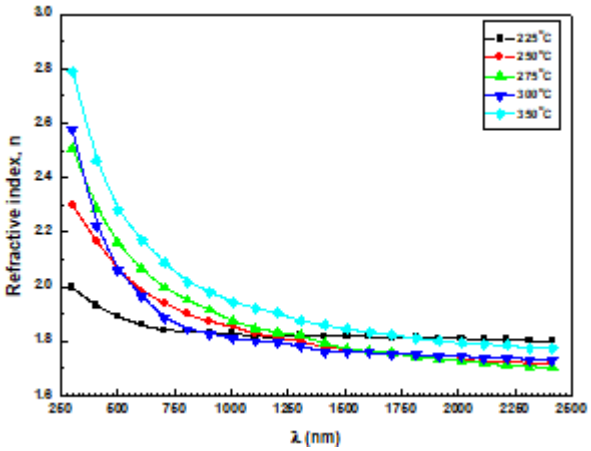

Figure 4: Refractive index, n as a function of wavelength, λ for different substrate temperatures of NiO thin films

Figure 4 shows the spectral variation of the refractive index, n as a function of wavelength at different substrate temperature. It can be seen that, the maximum value of refractive index (n=2.8 at T_{sub}=350°C) at very low wavelength, λ=300nm (strong-absorption region) was observed in all samples. This is due to the equality between the frequency of incident electromagnetic radiation and the frequency of electrons oscillation. This leads to the coupling of electrons in NiO films to the oscillating electric field. At longer wavelengths, λ>500nm, the refractive index is sharply decreasing for all patterns reaching to the lowest value of 1.8 at λ≥900nm and then the n value remains slightly changed for the whole wavelength. Furthermore, the behaviors of refractive index of all films are similar, which is due to the normal dispersion. In the NIR region, λ≥1000 nm, the n values differ slightly with substrate temperature then diverge remarkably in the visible region. These results are in good agreement with the data obtained by others [9] for like phase.

3.2.4 Extinction coefficient

The imagery part, k of the refractive index depends on the crystalline structure of the solid material. The behavior of waves within the solid matter (crystalline materials) are scattered between the crystalline agglomerations (particle size) of the material. Thus, the waves will be a random scattering inside the grain boundaries of solid materials. Therefore; the k value of was smaller. While, in the amorphous structure, the k value is higher. This is due to the occurrence of many irregular internal scattering and the absorption coefficient increases. Thus, the extinction coefficient k increases with both reduces of the wavelength (called absorption region) and in the amorphous materials (low aggregates) while the extinction coefficient, k, decreases with the crystalline agglomeration size increases (crystalline materials). The extinction coefficient k is estimated from the values of T and R as in the following equation;

$$k=\left(\frac{\lambda}{4\pi d}\right)Ln\left(\frac{1-R}{T}\right) \qquad \textbf{(6)}$$

The dependence of the extinction coefficient on the substrate temperature appears in Figure 5. It is evident that the extinction coefficient of the films decreased irregularly with an increase in substrate temperature. It can also be seen that for deposited films and those at lower substrate temperatures (225-275°C), the extinction coefficient decreased significantly, but for substrate height (275-350°C), the variance was slightly.

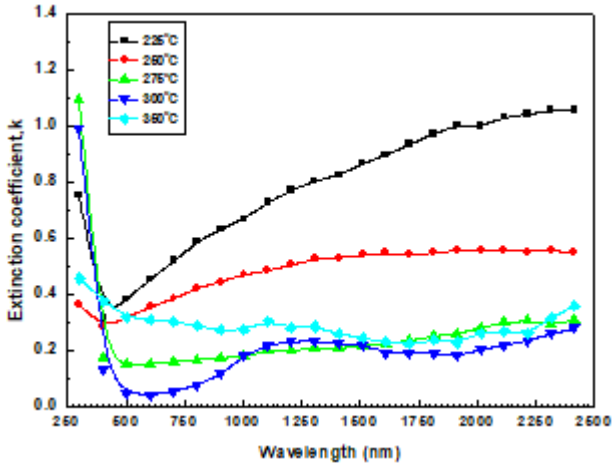

Figure 5: Extinction coefficient variation with wavelength of NiO thin films with different substrate temperatures

In order to interpreted this behavior must taking into account the microstructure parameters of the NiO thin films carried out from the XRD analysis. The structural phases change from amorphous to polycrystalline phases with substrate temperature increasing. Generally, the extinction coefficient is associated with absorption properties of the material. The lower transmittance (amorphous phases at low temperature) is not caused by the absorption but it is caused by the dispersion of light on quite large crystallites build in the amorphous matrix which has higher extinction coefficient than the polycrystalline phase [26].

3.2.5 Dielectric functions

From Maxwell's equations, propagation of a wave through a solid depends upon the dielectric constant (ε) that defines the magnitude of the displacement current due to the time variation of the applied field, and the conductivity (σ), which is a measure of the real current in the material that is created by the electric field. Therefore, the response of amorphous and crystalline phase to the incident electromagnetic radiation of very high frequency is through coupling of electrons in the material to the oscillating electric field. The dielectric function characterize the optical properties of any solid material and it is depends on the wavelength of light and the complex refractive index n* = n (λ) + ik (λ). The imaginary and real parts of dielectric constant were determined by the following relations, $\varepsilon_r^* = \varepsilon_{real}(\lambda) + i\varepsilon_{imag}(\lambda)$ in the absorption region (k (λ) ≠ 0). The relationship between the relative permittivity, ε_r and the electrical susceptibility, χ_e of non-polar particles in solids as follows [26-31];

$$\varepsilon_r = 1 + \chi_e = (1 + \chi_{real}) + i\chi_{imag} \quad (7)$$

$$n^{*2} = \varepsilon_r = (n^2 + k^2) + i(2nk) \quad (8)$$

Then

$$\chi_{real} = n^2 - k^2 - 1 \text{ And } \chi_{imag} = 2nk \quad (9)$$

The relation of the real dielectric constant as a function of the beam wavelength and the plasma frequency are as follows:

$$\varepsilon_{real} = \varepsilon_\infty(1) - \left(\frac{e^2}{4\pi^2 c^2 \varepsilon_o}\right)\left(\frac{N}{m^*}\right)\lambda^2 \quad (10)$$

and

$$\varepsilon_{real} = \varepsilon_\infty(1) - \frac{w_p^2}{w^2} = \varepsilon_\infty(1) - \frac{w_p^2}{4\pi^2 c^2}.\lambda^2 \quad (11)$$

Then

$$w_p = \frac{e^2}{\varepsilon_o}\left(\frac{N}{m^*}\right) \quad (12)$$

And

$$\varepsilon_{imag} = \chi_{imag} = \left(\frac{\varepsilon_\infty w_p^2}{8\pi^2 c^3 \tau}\right)\lambda^3 \quad (13)$$

Where, ε_{real} is the real part of the dielectric constant (represents the normal dielectric constant), ε_{imag} is the imaginary part of the dielectric constant (represents the absorption associated of radiation by free carrier), $\varepsilon_{\infty(1)}$ is the lattice dielectric constant (represents the normal dielectric constant), λ is the wavelength, N is the concentration of the free charge carrier, ε_o is the permittivity of free space, m* is the effective mass of the charge carrier, ω_P is the plasma frequency, τ is the optical relaxation time and c is the speed of light.

Electrical susceptibility, χ is one of the most important characteristics of materials that contain highly specific electrons, such as amorphous and other optical materials, which are insulating materials. However, the electrical susceptibility of the insulating material can be more appropriate than the refractive index to describe the light interaction with these materials. Measuring the material's ability to polarize can be transient. From optical constants, electric susceptibility (χ_{real}) can be calculated according to equation (9). Electrical susceptibility is a complex quantity because photon irradiation induces two independent physical responses in matter: dispersion, wavelength-dependent propagation of the beam through matter and absorption, transfer of radioactive energy to vibration energy in the material. Electrical susceptibility as a function of the photon energy of NiO films at different temperatures as shown in Figure 6.

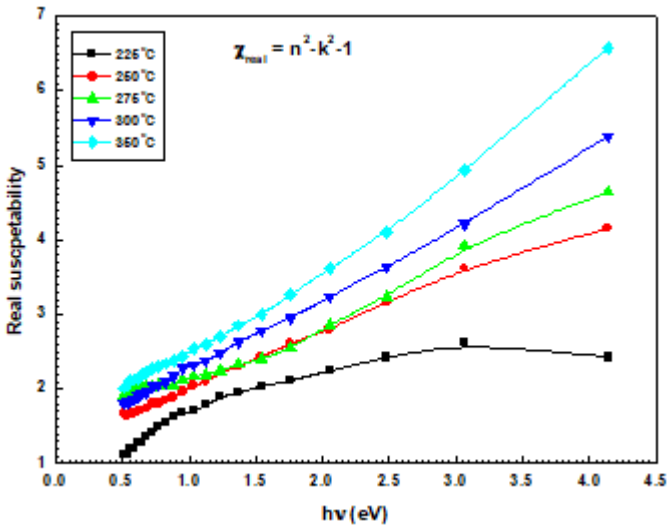

Figure 6: Electrical susceptibility as a function of photon energy for NiO thin films at different substrate temperature

It has been observed that the electrical susceptibility at high temperatures is greater than low temperatures because the heat improves the crystallization of the material. Therefore, the ability of the electric field diffused within the crystalline material has a greater ability to diffuse the amorphous materials. Because the process of diffusing of the electric field within the solids depends on the limits of agglomeration crystalline (grain boundary) in crystallized materials which is an increase of the electrical displacement.

The real and imaginary parts of the dielectric constant ε1 were calculated at different values of λ in the transparent region (at k = 0). Then, the values obtained from ε_{real} and ε_{imag} are drawn as a function of λ^2 from the NiO films as shown in the figures 7 and 8. It was observed that the dependence of ε_{real} and ε_{imag} on linear λ^2 at longer wavelengths (transparent region). The linear part of this dependence is extrapolated to zero wavelength $\varepsilon_\infty(1)$ and from the slope of this line can be calculated the N/m* and ω_p for NiO thin films according to equations(11 and 12). Table 1 shows the values obtained from $\varepsilon_\infty(1)$, ω_p and N/m*.

The dielectric relaxation time τ can be determined by the following equation [27, 32–34]:

$$\tau = \left|\frac{\varepsilon_\infty - \varepsilon_1}{\omega \varepsilon_2}\right| \quad (14)$$

The absolute value is taken for the equation (14) because the value of ε_∞ is always less than ε_1. Figure (9) depicts the

relaxation time of the τ as a function of photon energy for NiO films.

Table 1: The calculated values of the R_{RMS}, dielectric constant, ε_∞, N/m*, plasma frequency, w_p the dielectric relaxation time, τ and Urbach energy, E_U

Sample	R_{RMS} (nm)	ε_∞	N/m* x10^{56} ($gm^{-1}.cm^{-3}$)	w_p x10^{15} (Hz)	τ x10^{-19} (sec)	E_U(eV)	α_o x$10^4 cm^{-1}$
225°C	84.26	2.899	1.8096	5.2345	0.9234	0.6529	5.4086
250°C	70.55	3.101	1.4905	4.3114	1.0573	0.6250	7.9496
275°C	52.67	3.189	1.1229	3.2481	1.3566	0.5215	25.357
300°C	41.39	3.207	0.6266	1.9811	1.5275	0.4386	30.586
350°C	28.74	3.433	6.5033	1.8127	2.8017	0.3652	54.036

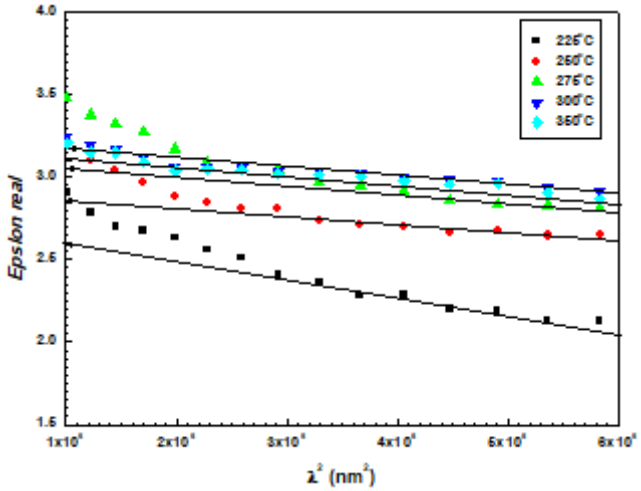

Figure 7: Variation of the real part of the dielectric constant, ε_{real} as a function in λ^2 of NiO thin films when temperatures change of substrate

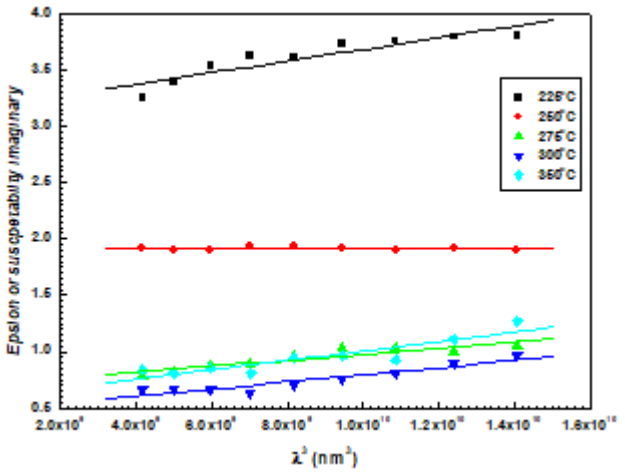

Figure 8: Variation of the imaginary part of the dielectric constant, ε_{imag} as a function in λ^2 of NiO thin films when temperatures change of substrate

The value of the relaxation time can be evaluated throughout this plot from the crossing point between the tangent of the plot of the lower and higher values of the photon energy at indicated the values of relaxation time on the y-axis. The estimated values for the relaxation time of NiO are recorded at the different substrate temperature in Table 1. The value of relaxation time is clearly decreasing at a higher temperature. Because intermediary vacancies were reduced between Ni atoms and O-atoms. This is due to the NiO films have improved crystallization at higher temperatures.

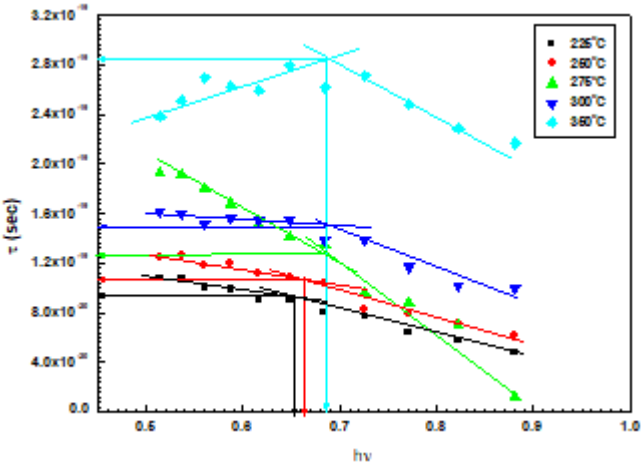

Figure 9: variation of the relaxation time, τ as a function of photon energy for NiO films.

3.2.6 Optical conductivity of NiO thin films

Semiconductor conductivity can be understood in the energy band model. At T=0K the valence band is completely filled and the conduction band is left empty. Thus, no free charge carriers, which can be accelerated by an applied electric field, are not available. Hence, when the temperature is zero, semiconductors are insulators. While, at a higher temperature, electrons from the valence band can be excited to the conduction band by absorbing thermal energy, which is now able to accelerate it by an external electric field. At the same time, lost electrons in the valence band by stimulating the electrons to the conduction band can act with positive charge (holes) that also contribute to the total conductivity. In addition, the electrical conductivity of thin semiconductor films increases with film thickness as long as and the electron collisions with the film surface are non-specular. The effect is important for films whose thickness is of the order of or less than the bulk mean free path of the conduction electrons. For a semiconductor with a spherical Fermi surface in which all electron scattering events are isotropic. The complex optical conductivity $\sigma^*=\sigma_1(\lambda)+i\sigma_2(\lambda)$ is related to the complex dielectric constant ($\varepsilon* = \varepsilon_1(\lambda) + i\varepsilon_2(\lambda)$) by the relation [27,35,36];

$$\sigma_1 = \omega\varepsilon_o\varepsilon_2 \text{ and } \sigma_2 = \omega\varepsilon_o\varepsilon_1 \quad (15)$$

The real σ_1 and imaginary σ_2 parts of the optical conductivity as a function of the photon energy are shown in Figures 10 & 11.

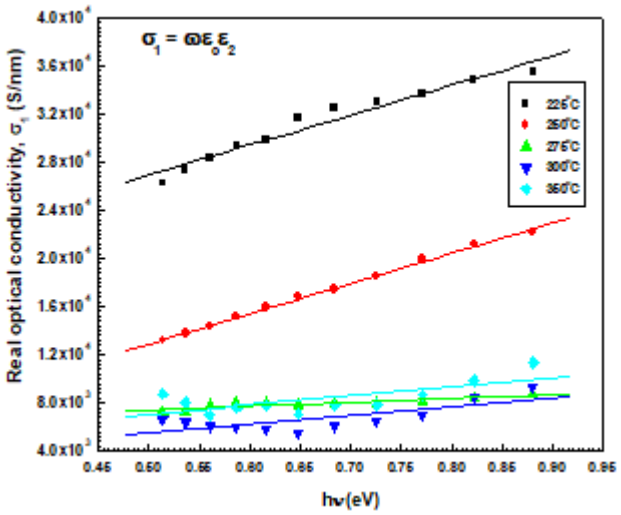

Figure 10: Dependence of the real part of the optical conductivity on the photon energy for NiO thin films at different temperature

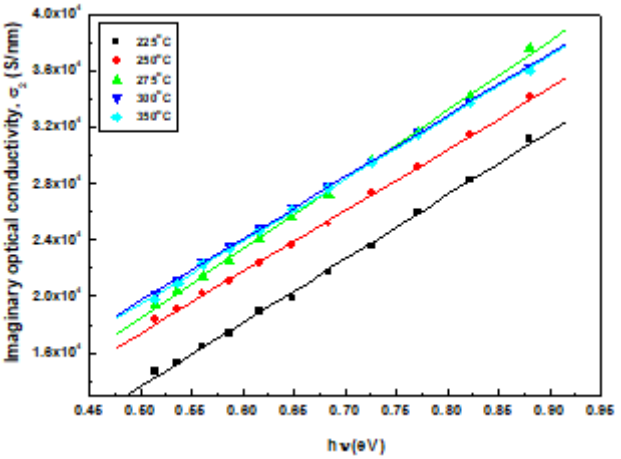

Figure 11: The imaginary part of the optical conductivity as a function in photon energy for NiO at different temperature

It is clear from the figures that the real part of optical conductivity decreases with increasing temperature while the imaginary part decreases with increasing temperature. This is due to the behavior of mobility of electrons within the solid (crystalline materials) which are scattering and collisions between the crystalline agglomerations (particle size) of the material. Thus, the mobility of electrons will be a random scattering inside the grain boundaries of solid materials. Therefore; the real part of the optical conductivity was reduced. Therefore, the optical conductivity decreases with the crystallization process of NiO thin films. While, at lower temperature (amorphous structure), the imaginary part of optical conductivity was a linear increases with the photon energy. This is due to the occurrence of many irregular internal scattering and the absorption coefficient increased. Therefore , the imaginary part of optical conductivity increases with both increment of the photon energy (called absorption region) and in the improving crystallinity (higher agglomerate of crystallite).

3.2.7 Width of the tail of localized states

One of the consequences of a long-range missing is the existence of beam tail states. Local fluctuations in the interatomic distances between the atoms and the bonding angles result in spatial fluctuations of the edges of the band. This leads to areas within the band, where charge carriers can be trapped. Various models were proposed to adopt and combine models successfully used to describe transport data from polycrystalline or pure amorphous material [26,30,37]. Near the optical band edge, the relationship between (α) and (hν) is known as Urbach empirical rule, which is given by this exponential equation:

$$\alpha = \alpha_o \exp(\frac{h\nu}{E_U}) \quad (16)$$

$$Ln\alpha = Ln\alpha_o + (\frac{h\nu}{E_U}) \quad (17)$$

Where α_o is constant, (hy) is an incident photon energy and the E_U is the width of the band tail (Urbach energy) for the localized states into the optical energy gap. For amorphous structure NiO thin films, the behavior of Ln (α) vs. hν is shown near the absorption edge in Figure 12. The inverted slope of the straight lines leads to the determination of the Urbach energy, E_U. The values obtained from the band tail width are tabulated in the Table 1. It was observed that E_U values increased from 0.653 to 0.365 eV with increasing substrate temperature. E_U behavior can be attributed to increasing the substrate temperature of a NiO matrix, leading to increased atoms and turbulent defects in structural bonding. Disorders and defects can be lead to localized states at or near the connection band level, which increases the band tail width E_U [38-41].

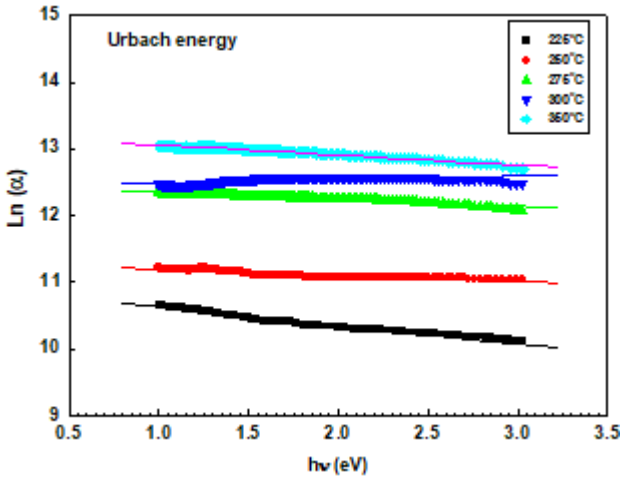

Figure 12: Urbach energy as a function of the photon energy for NiO at different temperature

3.2.8. Optical band gaps

The optical band gap was evaluated in the high absorption coefficient according to the function proposed by Tauc [26]:

$$\alpha(\nu)\, h\nu = B(h\nu - E_{gap})^m \quad (18)$$

where B is a parameter related to the semiconductor structural order, E_{gap} is the band gap of the material, hν is the energy and the exponent m determines the type of electronic transitions. To determine the accuracy of α, it is necessary to make corrections to absorbance due to reflection; also, m is the indicator which can be values different from 1/2, 3/2, 2, and 3 [30]. To introduce the absorption spectra fitting (ASF) method, one can begin with equation 2 and rewrite it as a function of the wavelength (λ):

$$\alpha(\lambda) = B(hc)^{m-1}\lambda(\frac{1}{\lambda} - \frac{1}{\lambda_g})^m \qquad (19)$$

where $C = B(hc)^{m-1}$, λ_g, h, and c are wavelengths corresponding to the optical band gap, Planck's constant, and velocity of light, respectively.

$$\frac{\alpha(\lambda)}{\lambda} = C(\frac{1}{\lambda} - \frac{1}{\lambda_g})^m \qquad (20)$$

$$\left[\frac{\alpha(\lambda)}{\lambda}\right]^{1/m} = \frac{C^{1/m}}{\lambda} - \frac{C^{1/m}}{\lambda_g} \qquad (21)$$

Using equation 21, one can calculate the optical band gap by absorption spectrum fitting method. Then the value of the band gap can be calculated in the electron volt of the λg parameter. In other words, the λg value can be the linear induction of the $(\frac{\alpha(\lambda)}{\lambda})^{1/m}$ = zero, curve versus 1/λ at when intercepting the y-axis. Using the least squares technique, it was observed that the best installation occurs for m = 1/2.

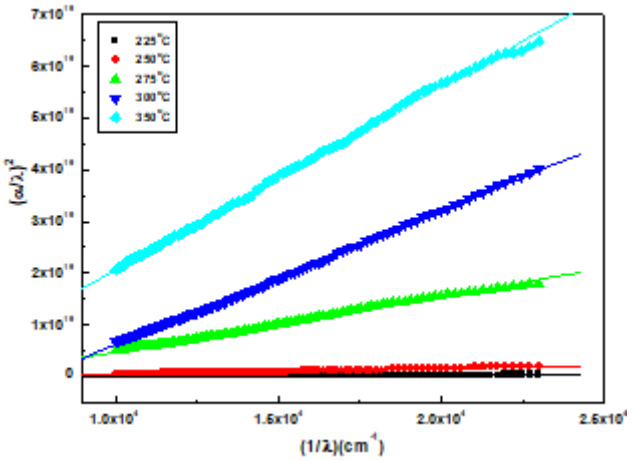

Figure 13: The relation between $(\alpha/\lambda)^2$ and $(1/\lambda)$ for NiO thin film at different temperature.

Table 2: The calculation optical energy gap values as a function of the substrate temperature for NiO thin films.

T_{sub}	Direct transition				Indirect transition	
(^oC)	B	C	λ_g(nm)	E_g(eV)	λ_g(nm)	E_g(eV)
225	$1.41x10^8$	$4.01x10^6$	332.1	3.738	444.89	2.790
250	$3.80x10^8$	$10.79x10^6$	348.3	3.564	530.68	2.339
275	$11.48x10^8$	$32.60x10^6$	361.4	3.435	566.36	2.192
300	$17.88x10^8$	$50.76x10^6$	388.3	3.197	591.80	2.097
350	$20.92x10^8$	$59.40x10^6$	394.5	3.146	605.72	2.049

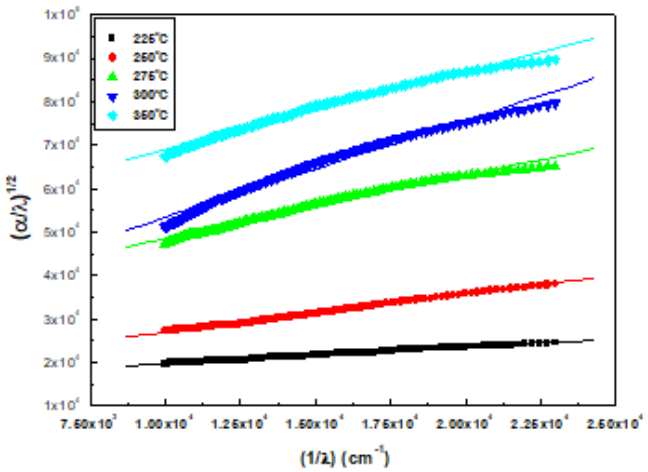

Figure 14: The relation between $(\alpha/\lambda)^{1/2}$ and $(1/\lambda)$ for NiO thin film at different temperature

Extrapolating the straight-line portion of the plots shown in Figure 13 to zero $(\frac{\alpha(\lambda)}{\lambda})^2$ gives the corresponding E_{gap} values (Table 2). The dependence of the optical gap on the deposition temperature for thin films is shown in Table 2. It is obvious that the optical gap is decreased by increasing the temperature because with increasing temperature, the crystallization of the NiO and crystallite size increases. Similarly, we can estimate the indirect transition from Figure 14, which is included in Table 2. These results were obtained for thin films NiO, a spectral behavior analysis that revealed direct and indirect allowed transitions [42-46].

4. Conclusions

The spray pyrolysis technique was used for depositing thin nickel oxide films on the heated glass substrate at the temperature of the substrate (T_{sub}) in the range of 225-350°C. XRD data reveals that, at lower temperature; NiO as amorphous structure; while at higher temperature (T_{sub} ≥275°C); NiO a single phase as a crystalline structure. Surface morphology using an AFM probe was detected in a morphological study observed that the co-ordination exercise of normal distribution was verified by observing the cumulative distribution of the surface. At lower T_{sub} (amorphous structure), optical absorption coefficient, α, is dominated by lower values, while at a higher, T_{sub}, (improve of crystalline degree), α in the whole wavelength pattern was higher. Where the skin depth is the reciprocal the alpha (Absorption coefficient) , then skin depth decreased with increased the agglomeration size. The maximum refractive index value at a very low wavelength, λ = 300 nm (strong absorption area) was observed in all samples. This is due to the equal frequency of electromagnetic radiation incident and frequency of oscillating electrons. The extinction coefficient k increases with both wavelength reduction (called absorption area) and non-crystallized material (low aggregate) while the extinction coefficient k decreases with increasing crystalline agglomeration (crystalline material). The real part of optical conductivity decreases with increasing temperature while the imaginary part decreases with increasing temperature. This is due to the behavior of the movement of electrons within the crystalline that are scattered and collide between the crystalline clusters

(particle size) of the material. Urbach energy behavior can be attributed to increasing the substrate temperature of the NiO matrix, leading to increased atoms and turbulent defects in structural bonding. It is clear that the optical energy gap (direct and indirect transition) decreases by increasing the temperature because as the temperature increases, crystallization of the NiO and crystallite size increased.

References

[1] D. Adler and J. J. Feinleib, Phys. Rev. B, 2 (1970) 3112.
[2] M. Zöllner, S. Kipp, and K. D. Becker, Cryst. Res. Technol., 35 (2000) 299.
[3] E.J.M. O'Sullivan, E.J. Calvo, in: R.G. Compton (Ed.), Compr. Chem. Kinet., 27 (1987) 274.
[4] C.M. Lambert, G. Nazri, P.C. Yu, Sol. Energy Mater., 16 (1987) 1.
[5] N. Shaigan, D.G. Ivey, W. Chen, J. Electrochem. Soc., 155 (2008) D278.
[6] K.K. Purushothaman, G. Muralidharan, J. Sol–Gel Sci. Technol., 46 (2008) 190.
[7] R. Cerc Korosec, P. Bukovec, B. Pihlar, A. Surca Vuk, B. Orel, G. Drazic, Solid State Ionics, 165 (2003) 191.
[8] B. Sasi, K.G. Gopalchandran, Nanotechnology, 18 (2007) 115613.
[9] H. Kamel, E.K. Elmaghraby, S.A. Ali, K. Abdel-Hady, Thin Solid Films, 483 (2005) 330.
[10] A. Mendoza-Galván, M.A. Vidales-Hurtado, A.M. López-Beltrán, Thin Solid Films, 517 (2009) 3115.
[11] I. Valyukh, S. Green, H. Arwin, G.A. Niklasson, E. Wäckelgård, C.G. Granqvist, Sol. Energy Mat. and Sol.Cells, 94 (2010) 724.
[12] M.A. Vidales-Hurtado, A. Mendoza-Galv´an, Materials Chemistry and Physics, 107 (2008) 33.
[13] E. Ozkan Zayim, I. Turhan, F.Z. Tepehan, N. Ozer, Solar Energy Materials and Solar Cells, 92 (2008)164.
[14] S.A. Mahmoud, A.A.Akl, H.Kamal, K.Abdel-Hady; Physica B, 311 (2002) 366.
[15] H.Kamal, E.K.Elmaghraby, S.A.Ali, K.Abdel-Hady; J. Crystal Growth, 262 (2004) 424.
[16] N.F. Mott, E.A. Davis, Electron processes in non-crystalline materials. Clarendon, Oxford (1979).
[17] A. Richter, S.A. Mahmoud and R. Ries, Vacuum, 66 (2002) 179.
[18] E.S. Gadelmawla, M.M. Koura, T.M.A. Maksoud, I.M. Elewa, H.H. Soliman, J. of Materials Processing Technology, 123 (2002) 133.
[19] O.S. Heavens, Optical Properties of Thin Films, Dover, New York, (1965).
[20] J.F. Eloy, Power Lasers National Sch. Phys., John Wiley and Sons, Grenoble, France, 1984.
[21] S.S. Chiad, Inter.letter Chem. Phys. Astro 6 (2015) 50.
[22] N.F. Habubi1, S.F. Oboudi, S.S. Chiad, J. Nano Electron. Phys. 4 (2012)4008.
[23] N.F. Mott, E.A. Davis, Electronic Processes in Non-Crystalline Materials, Clarendon, Oxford, 1979.
[24] S A. Mahmoud, S. M. Al-shomer and M. A. Tarawnh, Journal of Modern Physics, 2 (2011) 1178.
[25] C. Kittel , Introduction to Solid State Physics; 8th Edition; Wiley (1976).
[26] J. Tauc, A Menth, J Non-Cryst Solids, 569 (1972) 8.
[27] G.B. Sakr, I.S. Yahiaa, M. Fadel, S.S. Fouad, N. Romˇcevi´c, Journal of Alloys and Compounds, 507 (2010) 557.
[28] M. Fadel, S.A. Fayek, M.O. Abou-Helal, M.M. Ibrahim, A.M. Shakra, J. Alloys Compd., 485 (2009) 604.
[29] S.A. Khan, F.S. Al-Hazmi, S. Al-Heniti, A.S. Faidah, A.A. Al-Ghamdi, Curr. Appl. Phys., 10 (2010) 145.
[30] N. Chopra, A. Mansingh, GK. Chadha, J Non-Cryst Solids, 194 (1990) 126.
[31] A. El-Korashy, H. El-Zahed, M. Radwan, Physica B, 334 (2003) 75.
[32] J.N. Zemel, J.D. Jensen, R. B. Schoolar, Phys. Rev., A 140 (1965) 330.
[33] M.B. El-Den, M.M. El-Nahass, J. Opt. Laser Technol., 35 (2003) 335.
[34] M.G. Hutchins, O. Abu-Alkhair, M.M. El-Nahass, K. Abdel-Hady, Materials Chemistry and Physics, 98 (2006) 401.
[35] G.B. Sakr, I.S. Yahia, M. Fadel, S.S. Fouad, N. Romˇcevic´, Journal of Alloys and Compounds, 507 (2010) 557.
[36] F. Yakuphanoglu, M. Sekerci, O.F. Ozturk, Opt. Commun., 239 (2004) 275.
[37] A. Richter, R. Ries, Mol. Phys. Rep., 21 (1998) 11.
[38] A.S. Hassanien , Alaa A. Akl; Journal of Alloys and Compounds, 648 (2015) 280.
[39] S.A. Fayek, M. El-Ocker, A.S. Hassanien, Mater. Chem. Phys., 70 (2001) 231.
[40] C.M. Muiva, T.S. Sathiaraj, J.M. Mwabora, Eur. Phys. J. Appl. Phys., 59 (2012) 10301
[41] A. Sharma, N. Mehta, A. Kumar, J. Mater. Sci., 46 (2011) 4509.
[42] M.V. Kumar, S. Muthulakshmi, A. A. Paulfrit, J.Pandiarajan, N.Jeyakumaran, N.Prithivikumaran; Int. J. of ChemTech Res., 6, 13 (2014) 5174.
[43] M.M.El-Nahass, A.M. Farag, K.F. Abd El-Rahmann, A.A.A. Darwish ; *Opt. Laser Technol.* 37 (2005) 513.
[44] M. E. Sánchez-Vergara, J. C. Alonso-Huitron, A. Rodriguez-Gómez and J. N. Reider-Burstin; Molecules, *17* (2012) 10000.
[45] F. I. Ezema, A. B. C. Ekwealor, R. U. Osuji; J. of Optoelectronics and Advanced Materials, 9, 6 (2007)1898.
[46] M.Vignesh Kumar1, S. Muthulakshmi, A.Alfind Paulfrit,J.Pandiarajan, N.Jeyakumaran, N.Prithivikumaran; International Journal of ChemTech Research, 6, 13 (2014) 5174.